Contents lists available at ScienceDirect

Journal of Colloid and Interface Science

journal homepage: www.elsevier.com

Regular Article

Interactions of NIPAM nanogels with model lipid multi-bilayers: A neutron reflectivity study

Huihui Sun, Katarzyna Zielinska, Marina Resmini*, Ali Zarbakhsh*

Department of Chemistry, Queen Mary, University of London, Joseph Priestley Building, Mile End Road, London E1 4NS, United Kingdom

ARTICLE INFO

Article history:
Received 13 June 2018
Received in revised form 22 October 2018
Accepted 27 October 2018
Available online xxx

Keywords:
NIPAM nanogel
Lipid multi-bilayers
Interaction
Neutron reflectivity
Dermal drug delivery

ABSTRACT

In dermal drug delivery, the influence of the chemical structure of the carriers on their penetration mechanisms is not yet fully understood. This is a key requirement in order to design highly efficient delivery systems. In this study, neutron reflectivity is used to provide insights into the interactions between thermoresponsive *N*-isopropylacrylamide based nanogels, cross-linked with 10%, 20% and 30% *N,N'*-methylenebisacrylamide, and skin lipid multi-bilayers models. Ceramide lipid multi-bilayers and ceramide/cholesterol/behenic acid mixed lipid multi-bilayers were used for this work. The results indicated that in both multi-bilayers the lipids were depleted by the nanogels mainly through hydrophobic interactions. The ability of nanogels to associate with skin lipids to form water-dispersible complexes was found to be a function of the percentage cross-linker. An enhanced depletion of lipids was further observed in the presence of benzyl alcohol, a well-known skin penetration enhancer.

1. Introduction

Dermal delivery offers many potential benefits in pharmaceutical, dermatological, and cosmetic applications. In order to design and obtain efficient carriers for applications in dermal delivery, a greater understanding, at a molecular level, of the interactions and transport mechanisms across the skin barrier is essential [1–2]. Gel particles with cross-linked structures, in particular nanogels, have attracted interests as possible carriers. Nanogels have a high surface to volume ratio and the ability to form stable colloidal systems. Also they can be tailored through their chemical structure resulting in stimuli-responsive physicochemical properties [3–5]. They have been shown to respond to temperature, pH, ionic strength, presence of specific ions and redox conditions *etc*, by undergoing rapid conformational changes and altering their volume. These properties may offer outstanding advantages for applications in drug release.[6–9] Among the different type of matrices, thermo-responsive poly *N*-isopropylacrylamide (pNIPAM) nanogels, in particular, have attracted considerable interest because of their potential to be used as dermal drug delivery vehicles.[10–14] The linear pNIPAM has a lower critical solution temperature (LCST) of ~32 °C and the volume phase transition temperature (VPTT), at which its corresponding nanogels undergo shrinking/swelling behaviour, can be adjusted by incorporating different types and amounts of co-monomers and cross-linkers, based on target applications [15].

Although the route of penetration in dermal drug delivery is the subject of many studies [16–17], the intercellular hypothesis, where the drug moves through the lipid matrix of the stratum corneum (SC) is one of the commonly accepted one. The latter is known to display a multi-bilayer lamellar structure, mainly composed of ceramides, fatty acids, cholesterol and cholesterol sulphate [1–2]. There is considerable interests in developing experimental approaches that allow to prepare artificial systems that effectively mimic the skin barrier.

Solid supported lipid multi-bilayers can be prepared using a spin coating technique. Unlike the conventional methods, *e.g.* vesicle fusion, Langmuir-Blodgett and Langmuir-Schaeffer, spin coating technique offers the possibility to form a bilayer structure with a number of stacks [18] providing an idealised model for the skin lipid matrix structure.

Neutron reflectivity (NR) is a powerful technique for in situ characterization of supported lipid membrane systems [19–23] at interfaces because of its various advantages, e.g. a resolution of less than a nanometer, being non-destructive and capable of applying isotopic substitution which can be used for highlighting specific parts of the system [24]. Particularly, neutrons can be strongly scattered by elements constituting biological materials, such as carbon, hydrogen, nitrogen and oxygen.

We recently reported on the interactions between *N*-isopropylacrylamide nanogels (NI|PAM), cross-linked with 30% *N,N'*-methylenebisacrylamide (MBA), and model ceramide lipid monolayers at the air-water interface as a function of temperature [25], which were shown to be dominated by hydrophobic-hydrophobic binding. When a mixed ceramide/cholesterol/behenic acid monolayer was used, the interactions were strongly mediated by fatty acids. The data suggest

* Corresponding authors.
Email addresses: m.resmini@qmul.ac.uk (M. Resmini); a.zarbakhsh@qmul.ac.uk (A. Zarbakhsh)

https://doi.org/10.1016/j.jcis.2018.10.086
0021-9797/

Table 1
Theoretical scattering length density (*Nb*) of applied lipids, including the *Nb* of head group and tail group regions.

lipid name	ρ, g/cm^3	$Nb \times 10^{-6}$ Å^{-2}	head group $Nb \times 10^{-6}$ Å^{-2}	tail group $Nb \times 10^{-6}$ Å^{-2}
C16 ceramide (h-cer)	0.92	0.02	0.92	−0.15
cholesterol (h-chol)	1.02	0.21	0.78	0.20
behenic acid (h-BA)	0.83	−0.10	1.60	−0.36
benzyl alcohol	1.04	1.30	0.76	1.40

ρ - density, *Nb* - theoretical neutron scattering length density.

Table 2
Composition and characterisation of synthesized nanogels.

Sample	*Y*, %	d_h, nm	*PdI*	ρ, g/ml	VPTT, °C (±1.0)	$Nb \times 10^{-6}$ Å^{-2}
10% MBA	65	5.3±1.0	0.73	1.5	40	1.27
20% MBA	64	9.6±0.5	0.48	1.6	39	1.51
30% MBA	73	11.9±0.4	0.37	1.7	38	1.76

Y - polymerization yield, d_h - nanogel hydrodynamic diameter via volume determined by DLS , *PdI* - polydispersity index measured by DLS, ρ - density of dry nanogels. *PdI* scale 0–1.0 and *PdI* > *0.7* means a broad distribution of particle size. VPTT - volume phase transition temperature. Nb is the scattering length density for nanogels.

that the fluidity of the monolayer influences the interactions. In order to extend these simple models towards a more realistic system, given that the outer epidermal layer is surrounded by multiple layers of ceramide lamellae, we focused on multi-bilayer systems.

In this paper, we studied the interactions between NIPAM nanogels cross-linked with MBA (in molar ratios of 10, 20 and 30%) and two different lipid multi-bilayers; (i) pure ceramide lipid multi-bilayers and (ii) ceramide/cholesterol/behenic acid mixed lipid multi-bilayers. Penetration enhancers, which are capable of promoting the transport of active reagents across the skin barrier, are widely studied for dermal application [17,26]. The effect of the penetration enhancer benzyl alcohol on the interactions between nanogels and lipid multi-bilayers was also investigated.

2. Experimental section

2.1. Materials

N-isopropylacrylamide (NIPAM, 97%), *N,N′*-methylenebisacrylamide (MBA, 99%), anhydrous dimethyl sulfoxide (DMSO, 99.8%), cholesterol (99%), protonated behenic acid (99%), benzyl alcohol (C_7H_8O, with purity ≥99.8%) and D_2O (98 atom D %) were brought from Sigma Aldrich and used as provided. 2,2′-azobis(isobutyro)nitrile (AIBN, 98%, Acros) was recrystallized from methanol. Protonated *N*-palmitoyl-D-*erythro*-sphingosine (C16 ceramide lipid) was purchased from Avanti Polar Lipids, Inc. This ceramide was chosen as a means of continuity with our previous study where H and deuterated analogues of C16 ceramide were used for the study of interactions of ceramide with lipids at the air water interface [25].The ultrapure deionized water was prepared by the Purelab option water purification unit (Elgastat). Dialysis membranes (22 mm diameter, MWCO 3500 Da) were purchased from Medicell International Ltd. The silicon blocks which were used as the substrate for multi-bilayers were obtained from CRYSTRAN Ltd (Poole, Dorset UK).

2.2. Nanogel synthesis and characterization

Nanogels were synthesized via high dilution free radical polymerization, as previously reported [27]. NIPAM and MBA (in molar ratios of 10, 20 and 30%) were dissolved in a volume of DMSO to give a total monomer concentration (C_M) equal to 1%. Initiator AIBN (1% of total double bond molar concentration) was then added to the solution in a Wheaton bottle which was sealed, degassed and flushed with nitrogen to ensure the absence of any oxygen. The polymerisation was initiated at 70 °C (in thermostated oven) and carried out for 24 h. The clear solution was then dialyzed against deionized water for 2 days with frequent changes, followed by freeze drying (Labconco freeZone 6) which gave the nanogels as dry white powder. Dry nanogels were reconstituted by weighing and dissolving the material in the required solvent, followed by sonication for 2 min at room temperature and filtration of the solution through a Wheaton (PTFE) filter (0.45 µm).

The hydrodynamic diameters of nanogel particles were obtained from dynamic light scattering (DLS) data using a Zetasizer nano ZS (Malvern Instruments). The colloidal solutions (1.0 mg/mL) were filtered through a 0.45 µm syringe filter and were measured at 298 K (each measurement was repeated in triplicate).

The morphology of nanogels was further characterised by transmission electron microscopy, using a JEOL JEM 1230 (80 kV) instrument equipped with a camera from Morada. Following our previ-

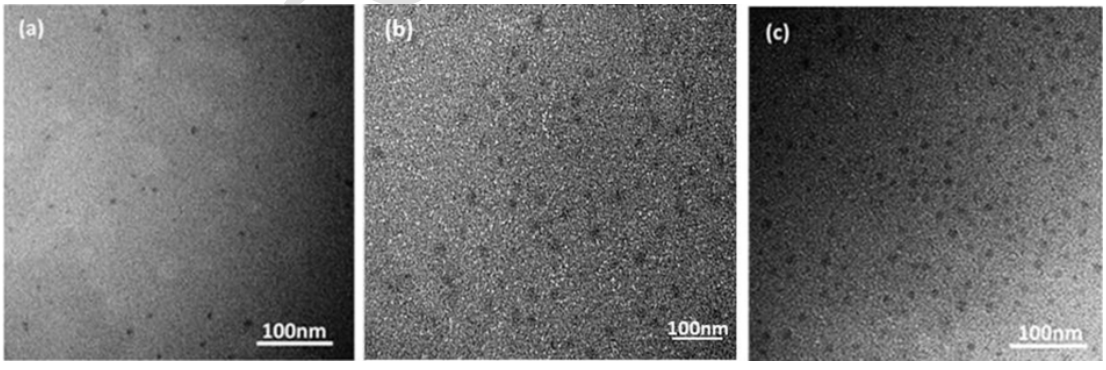

Fig. 1. TEM image of NIPAM nanogels containing (a) 10%, (b) 20% and (c) 30% MBA, obtained from graphene oxide support film without staining.

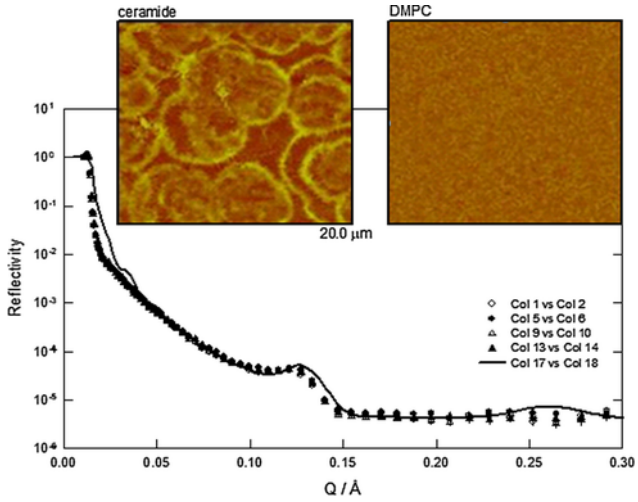

Fig. 2. Reflectivity spectra $R(Q)$ from the h ceramide lipid multi-bilayers at the Si-D_2O interface for a series of temperatures. The solid line is the fit to the data. AFM image of spun coated Si with asymmetric ceramide is shown. A comparable image for symmetric (even chain) 1,2-dimyristoyl-*sn-glycero*-3-phosphocholine (DMPC) devoid of any large domains is also shown.

Table 3
Parameters used for the fit to h ceramide lipid multi-bilayers at the Si-D_2O interface. The fit is shown by a solid line in Fig. 2.

	d, Å ±1.0	$Nb_{fitted} \times 10^{-6}$ Å^{-2} ±0.10	σ, Å	φ_{water}	N
head group region	4.0	2.20	1.0	24.0%	9
tail group region	43.0	0.90	1.0	16.0%	
head group region	4.0	2.20	1.0	24.0%	

d - thickness, Nb_{fitted} - fitted scattering length density (assuming the same density), σ – roughness, φ_{water} - volume fraction of water (D_2O), n - number of bilayers

ously published protocol,[28] the sample was prepared by pipetting 5 µL of nanogel dispersion (1.0 mg/mL) onto a copper grid (300 mesh) that has a graphene oxide support film on a lacy carbon backing, followed by drying in the air overnight.

The density (ρ) of the dry nanogel was estimated by measuring the volume, which was acquired from the difference of the helium pressure inside the empty chamber and the chamber filled with the nanogel of gas pycnometer AccuPyc 1330 (Micromeritics). The weight of the nanogel was determined using an analytical balance.

The volume phase transition temperatures (VPTTs) of nanogels in distilled water (at the concentration of 1.0 mg/mL) were determined by measuring the optical transmittance of the sample at $\lambda = 500$ nm over the temperature range 25 °C −60 °C. The spectrophotometer Cary 100 UV–vis (Agilent Technologies) that is equipped with an internal temperature controller was used. The optical path length of the sample was 10 mm and the temperature was raised at the constant rate of 1 °C/minute.

2.3. Lipid multi-bilayers preparation

The lipid multi-bilayers were deposited on the surface of single crystal silicon substrates. The silicon blocks were circular with a diameter of 100 mm and a thickness of 10 mm. In order to prepare the lipid multi-bilayers, the ceramide lipid or mixture of ceramide/cholesterol/behenic acid (molar ratio [29] 1:0.3:1) were dissolved in chloroform to make a solution with the concentration of 2.5 mg/mL. Approximately 250 µL of the solution was pipetted onto the RCA

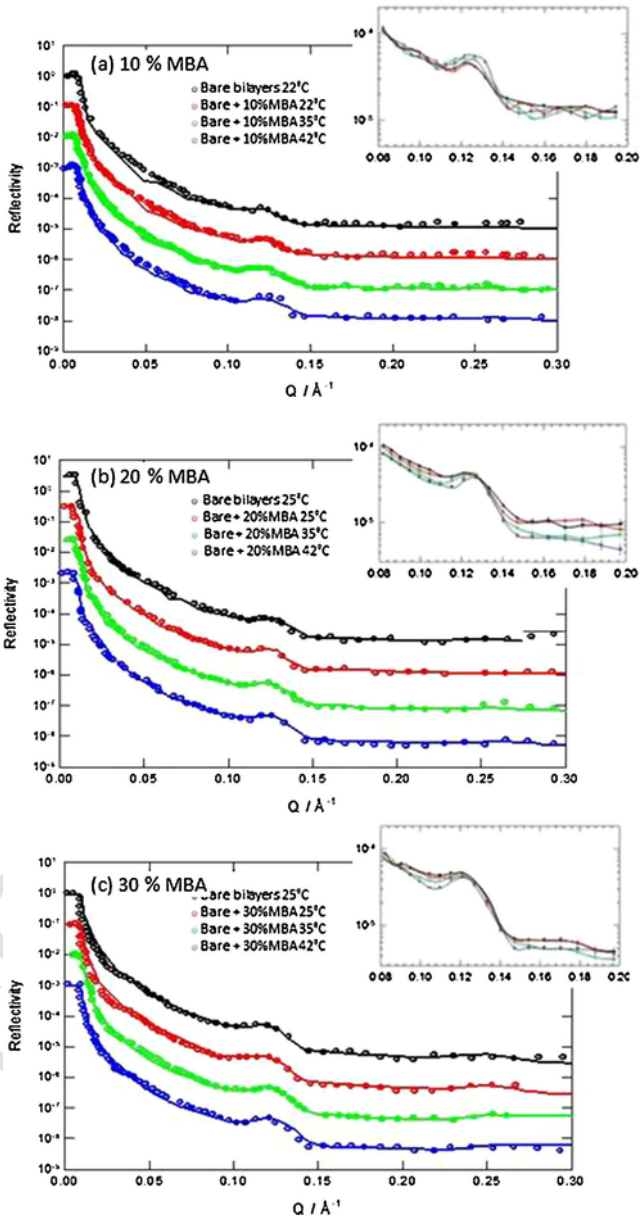

Fig. 3. Reflectivity spectra $R(Q)$ from the h-ceramide lipid multi-bilayers at the Si-D_2O interface for a series of temperature in the absence and presence of nanogels with (a) 10%, (b) 20% and (c) 30% MBA. The solid lines are the fits to the data. The insets show the changes in reflectivity profiles (markers + lines) upon addition of nanogels as a function of temperature.

[30] cleaned, hydrophilic pre-treated Si (1 1 1) substrate which was then spun at 1500 rmp for ~15 s using a programmable spin coater until all of the chloroform was evaporated.

2.4. Neutron reflectivity

Neutron reflectivity (NR) measurements were carried out at the ISIS Spallation Neutron Source, Rutherford Appleton Laboratory, Didcot, UK, using the SURF[31] and INTER[32] reflectometers. The reflectivity $R(Q_z)$ was measured using the time-of-flight technique as a function of momentum transfer normal to the interface $Q_z = (4\pi \sin \theta)/\lambda$, where λ and θ are the wavelength and the grazing angle of incident neutrons, respectively. The neutron beam on the instruments has

Table 4
Parameters used for fits to h-ceramide lipid multi-bilayers at Si-D_2O interface in the absence and presence of a) 10%, b) 20% respectively, as a function of temperature. The calculated fits are shown by solid lines in Fig. 3.

(a) 10% MBA

Temp, ±1 °C		d, Å ±1.0	$Nb_{fitted} \times 10^{-6}$ Å^{-2} ±0.1	σ, Å	φ_{water}	n
25 (bare multi-bilayers)	head group region	4.0	2.30	1.0	26.0%	5
	tail group region	39.0	1.40	1.0	24.0%	
	head group region	4.0	2.30	1.0	26.0%	
25 (multi-bilayers + 10% MBA)	head group region	4.0	2.30	1.0	26.0%	
	tail group region	39.0	1.40	1.0	24.0%	
	head group region	4.0	2.30	1.0	26.0%	
35 (multi-bilayers + 10% MBA)	head group region	4.0	2.65	1.0	31.0%	
	tail group region	39.0	1.50	1.0	25.0%	
	head group region	4.0	2.65	1.0	31.0%	
42 (multi-bilayers + 10% MBA)	head group region	4.0	2.80	1.0	35.0%	
	tail group region	39.2	1.60	1.0	27.0%	
	head group region	4.0	2.80	1.0	35.0%	

(b) 20% MBA

Temp, ±1 °C		d, Å	$Nb_{fitted} \times 10^{-6}$ Å^{-2}	σ, Å	φ_{water}	n
25 (bare multi-bilayers)	head group region	4.0	2.30	1.0	26.0%	6
	tail group region	39.2	1.40	1.0	24.0%	
	head group region	4.0	2.30	1.0	26.0%	
25 (multi-bilayers+20% MBA)	head group region	4.0	2.30	1.0	26.0%	
	tail group region	39.2	1.40	1.0	24.0%	
	head group region	4.0	2.30	1.0	26.0%	
35 (multi-bilayers+20% MBA)	head group region	4.0	2.50	1.0	29.0%	
	tail group region	39.2	1.60	1.0	27.0%	
	head group region	4.0	2.50	1.0	29.0%	

Table 4 (*Continued*)

(b) 20% MBA

Temp, ±1 °C		d, Å	$Nb_{fitted} \times 10^{-6}$ Å^{-2}	σ, Å	φ_{water}	n
42 (multi-bilayers+20% MBA)	head group region	4.0	2.70	1.0	33.0%	
	tail group region	39.2	1.75	1.0	29.0%	
	head group region	4.0	2.70	1.0	33.0%	

d - thickness, Nb_{fitted} - fitted scattering length density, σ – roughness, φ_{water} - volume fraction of water (D_2O), n - number of bilayers

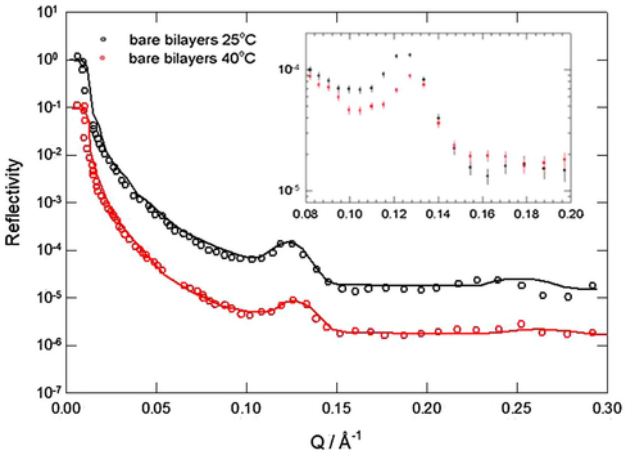

Fig. 4. Reflectivity spectra $R(Q)$ from the mixed lipid multi-bilayers at the Si-D_2O interface for a series of temperature. The solid lines are the fit to the data. The inset shows the changes in reflectivity profiles upon heating.

Table 5
Parameters used for fits to mixed lipid multi-bilayers at the Si-D_2O interface at different temperatures. The calculated fits are shown by solid lines in Fig. 4.

Temp, ±1 °C		d, Å ±1.0	$Nb_{fitted} \times 10^{-6}$ Å^{-2} ±0.10	σ, Å	φ_{water}	n
25	head group region	4.0	2.20	1.0	20.0%	20
	tail group region	41.0	0.90	1.0	17.0%	
	head group region	4.0	2.20	1.0	20.0%	
40	head group region	4.0	2.70	1.0	31.0%	
	tail group region	40.0	1.80	1.0	30.0%	
	head group region	4.0	2.70	1.0	31.0%	

d - thickness, Nb_{fitted} - fitted scattering length density, σ – roughness, φ_{water} - volume fraction of water (D_2O), n - number of bilayers

a wavelength of 0.5 Å < λ < 6.5 Å for SURF and of 1.5 Å < λ < 20.0 Å for INTER. In order to obtain the widest Q range and the highest sensitivity to interfacial structure, reflectivity spectra were measured for

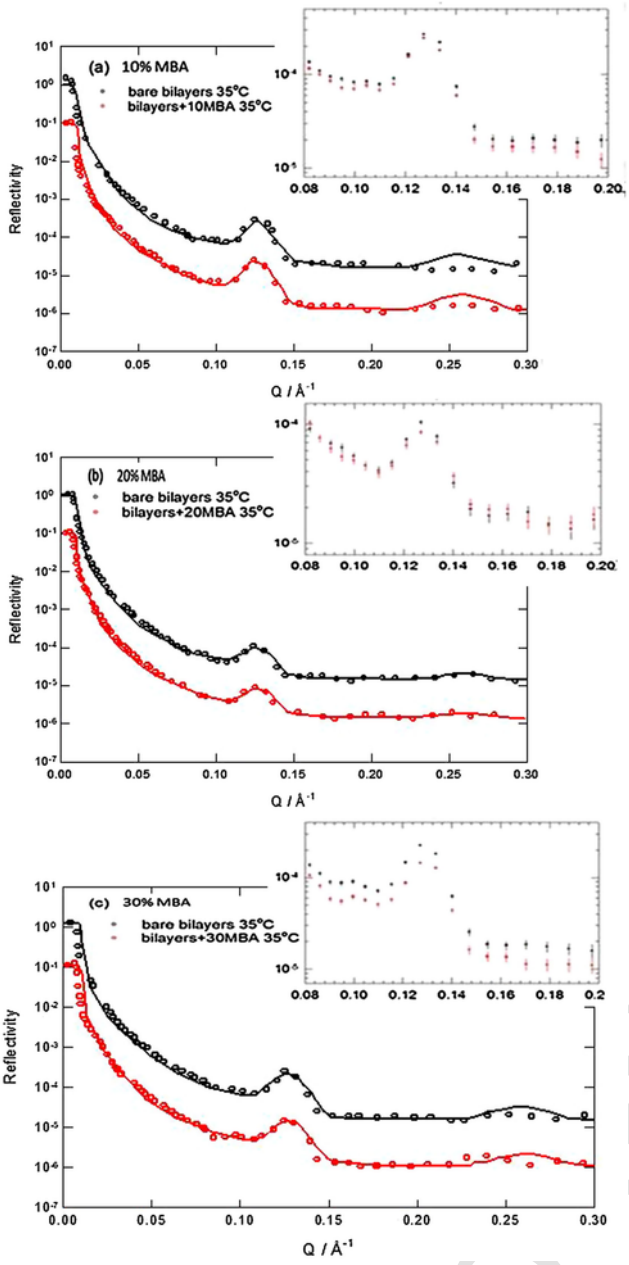

Fig. 5. Reflectivity spectra *R(Q)* from the mixed lipid multi-bilayers at the Si-D_2O interface at 35 °C in the absence and presence of nanogels with (a) 10%, (b) 20% and (c) 30% MBA. The solid lines are the fits to the data. The insets show the changes in reflectivity profiles upon addition of nanogels.

a series of grazing incidence angles θ. The nominal incidence angles used were 0.35°, 0.8°, and 1.8° for SURF or 0.7° and 2.3° for INTER. The sample was under illuminated with resolution $dQ/Q \sim 3\%$.

The contrast chosen for these experiments was Si/h-ceramide/D_2O for pure ceramide lipid multi-bilayers, and Si/(h-ceramide/h-cholesterol/h-behenic acid)/D_2O for mixed lipid multi-bilayers. Once the multi-bilayers were deposited, the Si block was placed on a solid-liquid trough and then the bulk aqueous solution was then gently injected to expel the air and fill the trough. The schematic diagram of the sample trough is shown in Fig. S1. The thermo-stabilities of the two bare multi-bilayers were first examined prior to the interaction studies. Then a known amount of nanogels were injected underneath the newly formed multi-bilayers (final nanogel bulk concentration in the sample trough 0.005 mg/mL) The effect of the enhancer on the interaction was subsequently examined by injecting the benzyl alcohol (the same amount as nanogel) into the sample trough and measuring the neutron reflectivity profiles as a function of time. The reflectivity of lipid multi-bilayers only in the presence of benzyl alcohol was also measured at the same temperature as a function of time. All the NR measurements were performed after allowing the system to equilibrate for ~30 mins after the injection of either nanogels or benzyl alcohol. The measured reflectivity profiles were corrected for the wavelength-dependent transmission through the silicon substrate. The scattering length densities *Nb* can be written [33] as

$$Nb = \sum_i \varphi_i Nb_i \quad (1)$$

where φ_i and Nb_i are the volume fraction and scattering length density of component *i*, respectively. The sum of the volume fractions for all the species is 1 ($\sum_i \Phi_i = 1$). The *Nb* of both head group and tail group of the lipids used for these experiments are shown in Table 1.

3. Results and discussion

3.1. Nanogel characterisation

A series of NIPAM nanogels with different percentage of cross-linker (MBA) were synthesized via high dilution free radical polymerization, a method which is capable of providing effective control over the particle size and the degree of polydispersity without the need for surfactants [32,33]. As it can be seen in Table 2, the nanogels were obtained with good chemical yields. NMR studies were conducted to confirm complete monomer conversion under the experimental conditions used. The lower chemical yields are the result of loss of low molecular weight polymer particles during the dialysis step, used for the nanogel purification. The size of the nanogels was found to be between 5 nm and 12 nm, consistent with our previous data. These values are noticeably smaller compared with those previously reported [12–13,34], mainly as a result of the synthetic methodology used (high dilution radical polymerization). The prepared nanogels have a roughly spherical shape as shown by the TEM images (Fig. 1). The solvated nanogels were placed on the support film and then the solvent was allowed to evaporate. Consequently, the structure of dehydrated nanogels was in a collapsed and expanded '2D conformation' for TEM studies and a larger size was observed. As a result, a small amount of aggregates with larger size can also be observed in the images, highlighted by the white boxes in Fig. 1. The observed average size and trend are consistent with the DLS measurement, in spite of the existence of the small amount of aggregates (see Fig. 1b). The values of polydispersity index (*PdI*) of nanogel particles were also determined by DLS and the results indicate that the particles with larger amounts of cross-linker tend to have a narrower size distribution. The correlation of data on particle size and *PdI* with the percentage of cross-linker suggests an important role that cross-linker plays in the polymerization process. The increase in cross-linker content provides a more compact nanoparticle with an extended three dimensional matrix (large particle size and higher density), with a tendency to form well-defined globular structures.

Table 6
Parameters used for the fitting to mixed lipid multi-bilayers at the Si-D_2O interface in the absence and presence of (a) 10%, (b) 20%, (c) 30% MBA, respectively, at 35 °C. The calculated fits are shown by solid lines in Fig. 5.

(a) 10% MBA						
Sample		d, Å ±1.0	$Nb_{fitted} \times 10^{-6}$ Å^{-2} ±0.1	σ, Å	φ_{water}	n
bare multi-bilayers	head group region	4.0	2.20	1.0	20.0%	38
	tail group region	40.0	0.90	1.0	17.0%	
	head group region	4.0	2.20	1.0	20.0%	
multi-bilayers + 10% MBA	head group region	4.0	2.25	1.0	21.0%	
	tail group region	40.0	1.05	1.0	19.0%	
	head group region	4.0	2.25	1.0	21.0%	
(b) 20% MBA						
Sample		d, Å ±1.0	$Nb_{fitted} \times 10^{-6}$ Å^{-2} ±0.1	σ, Å	φ_{water}	n
bare multi-bilayers	head group region	4.0	2.70	1.0	30.0%	22
	tail group region	40.0	1.70	1.0	29.0%	
	head group region	4.0	2.70	1.0	30.0%	
multi-bilayers+20% MBA	head group region	4.0	2.80	1.0	31.0%	
	tail group region	40.0	1.90	1.0	32.0%	
	head group region	4.0	2.80	1.0	31.0%	
(c) 30% MBA						
Sample		d, Å ±1.0	$Nb_{fitted} \times 10^{-6}$ Å^{-2} ±0.1	σ, Å	φ_{water}	n
bare multi-bilayers	head group region	4.0	2.20	1.0	20.0%	31
	tail group region	40.0	0.90	1.0	17.0%	
	head group region	4.0	2.20	1.0	20.0%	
multi-bilayers+30% MBA	head group region	4.0	2.50	1.0	27.0%	
	tail group region	40.0	1.50	1.0	26.0%	
	head group region	4.0	2.50	1.0	27.0%	

d - thickness, Nb_{fitted} - fitted scattering length density, σ – roughness, φ_{water} - volume fraction of water (D_2O), n - number of bilayers

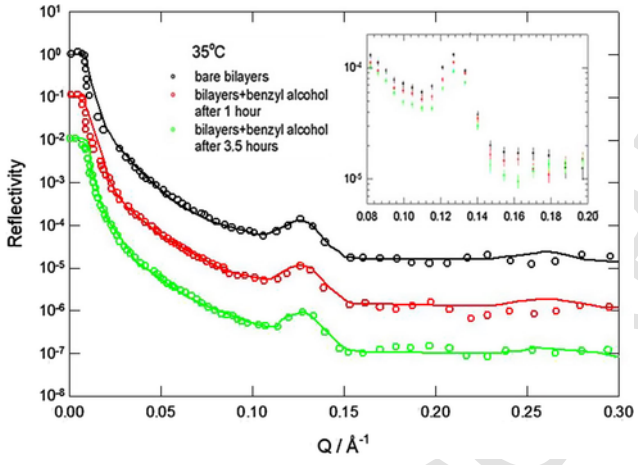

Fig. 6. Reflectivity spectra $R(Q)$ from the mixed lipid multi-bilayers at the Si-D_2O interface at 35 °C in the absence and presence of benzyl alcohol measured after 1 h and 3.5 h, respectively. The solid lines are the fits to the data. The inset shows the changes in reflectivity profiles upon addition of benzyl alcohol as a function of time.

4. Interaction of nanogels with lipid multi-bilayers

4.1. The structure and thermo-stability of pure ceramide lipid multi-bilayers

The neutron reflectivity profile of bare h-ceramide lipid multi-bilayers at the Si-D_2O interface was measured as a function of temperature in order to study their thermo-stability. The overlapped profiles (Fig. 2) suggest that the ceramide lipid multi-bilayers are stable over the temperature range of 25 °C–42 °C; this is in agreement with the results obtained with its monolayer counterpart at the air-water interface.[25] The presence of a Bragg peak indicates the formation of stacks of bilayers and the periodicity d of the bilayers is determined

Table 7
Parameters used for fits to reflectivity profiles from mixed lipid multi-bilayers at the Si-D_2O interface at 35 °C in the absence and presence of benzyl alcohol measured after 1 h and 3.5 h respectively. The calculated fits are shown by solid lines in Fig. 6.

Sample		d, Å ±1.0	$Nb_{fitted} \times 10^{-6}$ Å^{-2} ±0.1	σ, Å	N
bare multi-bilayers	head group region	4.0	2.20	1.0	17
	tail group region	40.0	0.90	1.0	
	head group region	4.0	2.20	1.0	
multi-bilayers + benzyl alcohol after 1 h	head group region	4.0	2.27	1.0	
	tail group region	40.0	1.10	1.0	
	head group region	4.0	2.27	1.0	
multi-bilayers + benzyl alcohol after 3.5 h	head group region	4.0	2.40	1.0	
	tail group region	40.0	1.35	1.0	
	head group region	4.0	2.40	1.0	

d - thickness, Nb_{fitted} - fitted scattering length density, σ – roughness, n - number of bilayers

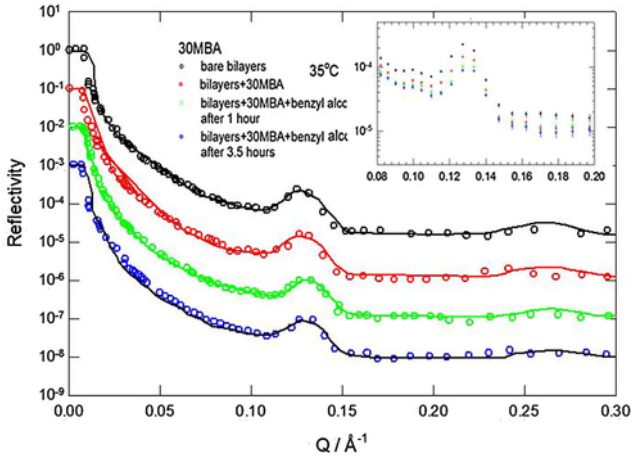

Fig. 7. Reflectivity spectra *R(Q)* from the mixed lipid multi-bilayers at the Si-D_2O interface at 35 °C in the presence of nanogel 30% MBA and benzyl alcohol. The solid lines are the fits to the data. The inset shows the changes in reflectivity profiles upon addition of benzyl alcohol as a function of time in presence of nanogel 30% MBA.

Table 8
Parameters used for fits to reflectivity profiles from mixed lipid multi-bilayers at the Si-D_2O interface at 35 °C in the presence of 30% MBA and benzyl alcohol. The calculated fits are shown by solid lines in Fig. 7.

Sample		d, Å ±1.0	$Nb_{fitted} \times 10^{-6}$ Å^{-2} ±0.1	σ, Å	N
bare multi-bilayers	head group region	4.0	2.20	1.0	31
	tail group region	40.0	0.90	1.0	
	head group region	4.0	2.20	1.0	
multi-bilayers + 30% MBA	head group region	4.0	2.50	1.0	
	tail group region	40.0	1.50	1.0	
	head group region	4.0	2.50	1.0	
multi-bilayers + 30% MBA + benzyl alcohol after 1 h	head group region	4.0	2.70	1.0	
	tail group region	40.0	1.80	1.0	
	head group region	4.0	2.70	1.0	
multi-bilayers + 30% MBA + benzyl alcohol after 3.5 h	head group region	4.0	2.90	1.0	
	tail group region	40.0	2.10	1.0	
	head group region	4.0	2.90	1.0	

d - thickness, Nb_{fitted} - fitted scattering length density, σ – roughness, n - number of bilayers

by the position of the Bragg peak (Q_d) according to Eq. (2):[35]

$$d = \frac{2\pi}{Q_d} \quad (2)$$

(Q is the scattering wave-vector ($Q = 4\pi \sin\Theta/\lambda$ where Θ is the angle of neutron beam incident and is λ the neutron wavelength). The periodicity d of the obtained multi-bilayers is calculated to be 52.0 Å ($Q_d = 0.12$ Å^{-1}). The width of the Bragg peak is indicative of the total layer hence by fitting the position of the number of periodicity n is obtained. Reflectivity data are analysed by model-fitting. The calculated reflectivity from the perpendicular refractive index profile is compared to the experimental data. The reflectivity data were fitted with a model consisting of homogeneous bilayers, where the thickness, *Nb* and roughness of each bilayer were kept constant across the sample.

In neutron reflectivity it is important to minimise the number of fitted parameters as much as possible in order to obtain a unique fit to the data. In our modelling (fitting), for example, the layer thicknesses deduced prior to nanogels injection were comparable to the molecular dimensions of the lipids used; hence these were fixed. The prominent (only) values which were allowed to vary were the scattering length density of the layers. This facilitates the changes in density (structure, water voids, diffusion of nanogels) to be resolved consistently.

The best fit to the profiles is shown by the solid line in Fig. 2. The corresponding *Nb* profile is shown in Fig. S2. The parameters used to fit the profiles are given in Table 3.

The total numbers of bilayers were found to be nine, with the thickness of the head group region equal to 4.0 Å and that of the tail group region being 21.5 Å. The periodicity of multi-bilayers determined by the fitting (51.0 Å) is close to the value determined by the position of the Bragg peak (~52.0 Å). It is worth noting that the thickness of half a bilayer (25.5 Å) is slightly larger than the length of an extended ceramide molecule (23.0 Å), which implies a poor ordering of the lipid molecules in the bilayer. The ceramides are most probably staggered (poorly aligned) with respect to each other because of the asymmetric nature (uneven tails) of their structure, which results in an in-plane inhomogeneity in the bilayers. This is further demonstrated by the higher background observed in the reflectivity data compared with the calculated reflectivity (Fig. 2). A parallel AFM study clearly showed the presence of large domains ~9 μm (in-plane structure) for spun coated ceramide multi-bilayers, however much smaller domain structures were observed for the symmetric (even chain) 1,2-dimyristoyl-*sn-glycero*-3-phosphocholine (DMPC), which was prepared for comparison,. This is in agreement with published literature using AFM, suggesting that defects are present in the structure of lipid multi-bilayers prepared by spin coating technique.[36] However these structural conformations observed for ceramides have not been reported previously and need further investigation. The *Nb* of the head group and tail group of the ceramide lipid molecule are 0.92×10^{-6} Å^{-2} and -0.15×10^{-6} Å^{-2} respectively (Table 1). The water contents of the head group and tail group regions of the multi-bilayers are estimated to be 24% and 16% respectively (Eq. (1)).

It is noticeable that the calculated reflectivity (black solid line, Fig. 2) exhibits some small Kiessig fringes below 0.1 Å^{-1} which are not observed experimentally. The presence of Kiessig fringes, which are the oscillations between the total reflection region and the Bragg peak, indicates a well-defined uniform film and the number of oscillations determines the number of bilayers [18,37]. The absence of the Kiessig fringes in the experimental profiles support the notation of a lack of long range order for the deposited ceramide bilayers. The ab-

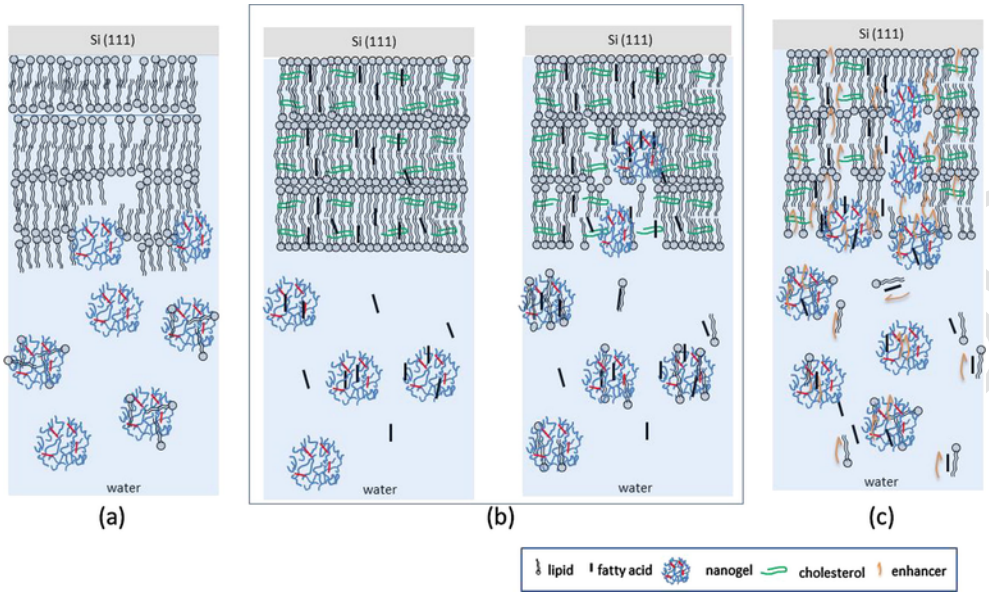

Fig. 8. Schematic diagrams show: (a) pure ceramide lipid multi-bilayers with defects and the subsequent solubilisation by nanogels resulting in diffusion of nanogels into multilayers. (b) the cholesterol providing structural rigidity with some fatty acids in bulk water as observed previously [25] forming a complex structure with nanogels. The solution and diffusion of nanogels into the lipids structure then follows. (c) the enhancer results in further solubilisation of lipids hence enhanced diffusion of nanogels into the lipid multilayers.

sence of the Kiessig fringes in the measured reflectivity profiles was, however, expected as the profiles measured are averaged over a large beam foot-print (~130 cm^2). The absence of a clear second order peak in the NR profiles (Fig. 2) at ~0.24 $Å^{-1}$ also indicates a poorly-ordered layered structure. This can explain the presence of small amounts of water (16%) found in the hydrophobic tail region. These results are in good agreement with published literature[38] which reports that ceramides alone do not exhibit a long range ordered structure. The presence of the well-defined Bragg peak (q_b=0.12 $Å^{-1}$) indicates that the internal structure at a small scale is relatively well defined.

4.2. Interaction of nanogels with pure ceramide lipid multi-bilayers

The next step focused on the study of the interaction of the nanogels with h-ceramide lipid multi-bilayers, which were freshly deposited each time. Nanogels with different crosslinker (MBA) content (10%, 20% and 30%) were injected carefully into the solid-liquid cell sample trough, and the interactions were studied as a function of temperature from 25 to 42 °C. The normalized NR data are shown in Fig. 3. The insets illustrate that the addition of nanogels results in increases in reflectivity, which also increases as the temperature is raised. Since pure ceramide lipid multi-bilayers are stable with temperature, these changes in the NR profiles are the result of the interactions between nanogels and the ceramides. The same model, which was used for the fitting of NR profiles of bare h-ceramide lipid multi-bilayers before the addition of nanogels, was used to represent the datasets in Fig. 3. The changes in the layer thickness (*d*) and the scattering length density *Nb* were then fitted. The best fits to the data are shown by solid lines in Fig. 3. The corresponding *Nb* profiles are shown in Fig. S3. The parameters used to fit the profiles are given in Table 4 for 10 and 20% MBA (Table S1 for 30% MBA). At 25 °C, the *Nb* of bilayers shows an increase only in the presence of 30% MBA nanogels, indicating the pronounced interaction of this nanogel with ceramide lipids.

After the temperature is increased to 42 °C, the *Nb* of the head group and tail group regions for the three nanogels increased from 2.30×10^{-6} $Å^{-2}$ & 1.40×10^{-6} $Å^{-2}$ to 2.80×10^{-6} $Å^{-2}$ & 1.60×10^{-6} $Å^{-2}$ for the 10% MBA nanogels, to 2.70×10^{-6} $Å^{-2}$ & 1.75×10^{-6} $Å^{-2}$ for the 20% MBA nanogels and to 3.15×10^{-6} $Å^{-2}$ & 2.15×10^{-6} $Å^{-2}$ for the 30% MBA (see Table 4 and S1). The water contents of the head group and tail group regions at different temperatures for the three samples are calculated according to Eq. (2) and shown in Table 4. The increase in *Nb* indicates the penetration of water (D_2O) in the bilayers. Consistent with the previous monolayer studies [25], the diffusion loss of the ceramide lipids by nanogels at the bilayer water interface results in water dispersible nanogel-lipid complexes. These results in the growth of defects in the bilayers, which then facilitates the further penetration of water into the bilayer structure and growth of exiting defects in the structure. These result in the enlargement of existing defects, providing a pathway for further nanogel penetration into the bilayers.

At each temperature, the water content of bilayers increases in line with higher percentage of crosslinker, as seen in Table 4 (and Table S1). At 42 °C, the water contents of head group and tail group regions increase by 9% and 3% in the presence of 10% MBA, 7% and 5% with 20% MBA nanogels and 16% and 12% with 30% MBA nanogels respectively. The data provide evidence of the ability of nanogels to deplete ceramide lipids; the variation in water contents can be justified by the difference in crosslinker content, which impacts structural rigidity and hydrophobicity of the matrix. The results suggest that nanogels with higher crosslinker content are better at depleting ceramide lipids. It is important to note that these experiments were carried out at a very low concentration of nanogels (0.005 mg/mL) and therefore all nanogel dispersions, regardless of the percentage of cross-linker, were in a state of colloidal stability (*i.e.* homogenous) over the investigated temperature range (25 °C–42 °C), which was confirmed by UV–VIS data. Hence, it is safe to state that the variation in VPTT values of these nanogels with different percentages of cross-linker is not a significant factor influencing the interactions. The increased structural rigidity due to higher crosslinker content, which results in nanogels with a higher degree of hydrophobicity [39], facilitates the interactions between the nanoparticles and the lipids, leading to increased depletion. This is consistent with the observation that lipid depletion is increased with temperature, as the

nanogels become more hydrophobic. Thus, *Nb* values of both head group and tail group regions increase with increasing temperature (see Table 4 and S1).

It is noteworthy that after the addition of 30% MBA nanogels the thickness of the tail group region of the bilayer gradually decreases from 41.5 Å to 40.8 Å with increasing temperature. This decrease, although small for each bilayer, nonetheless has a strong influence on the quality of the fit when the fit is calculated for the whole multi-bilayer stack. This is because increasing amounts of lipids are depleted as temperature increases, hence there is a growing scale of defects which allows for an increasing degree of freedom for the lipids to change their conformation to minimise the free energy. A smaller layer thickness to form the fits suggests mixed/interdigitated states of the lipids. This phenomenon was not observed for the other two nanogels. This could be because of a smaller degree of lipids depletion and therefore the layers are still in a relatively better compact formation which reduces the ability of lipids to change their conformations.

4.3. The thermo-stability of mixed ceramide/cholesterol/behenic acid multi-bilayers

In order to obtain a representation that more closely matches the composition of skin, the mixture of ceramide/cholesterol/behenic acid (molar ratio 1: 0.3: 1) was used to form the multi-bilayers. The thermo-stability of this mixed lipid multi-bilayer was first examined by NR. The normalized NR profiles as a function of temperature are shown in Fig. 4. The variation in the NR profiles suggests the mixed lipid multi-bilayers are not stable with increasing temperature, in contrast to the pure ceramide multi-bilayers. The reason for this is because of the decrease in the lateral intermolecular forces and increase fluidity of the ceramide lipid multi-bilayers upon addition of cholesterol and behenic acid. This result is consistent with that obtained from the ceramide lipid monolayer study [25].

The best fits to the profiles are shown by solid lines in Fig. 4. The corresponding scattering length density profiles are shown in Fig. S4. The fitted parameters used are given in Table 5. Compared with pure ceramide lipid multi-bilayers at 25 °C, the Bragg peak of the mixed lipid multi-bilayers is sharper which is indicative of the formation of a much better ordered lamellar structure as expected now in the presence of cholesterol. This can also be inferred by the goodness of the fit to the data. The fits indicate a greater number of bilayers (20) were formed compared with the pure ceramide counterpart (<10). The NR shows that the introduction of cholesterol and fatty acid results in an increased ordering of the ceramide molecules and thereby a much better ordered multi-bilayer structure. This conclusion is in good agreement with published literature [37] which reports that the lamellar phases are formed upon the addition of cholesterol to ceramide lipids. At 25 °C, the periodicity of the bilayers determined by the position of the Bragg peak (49.8 Å) is in good agreement with the value determined by the fitting (49.5 Å). The lengths of fully extended C16 ceramide, cholesterol and behenic acid are 23.0 Å, 18.0 Å and 28.0 Å respectively. The thickness of one bilayer is smaller than the length of two fully extended behenic acid molecules (56 Å) which act as the determinant of the bilayer thickness. This means that the molecules either intermix or more likely, they are tilted (28°) from the normal to the interface.

Assuming a uniform distribution of the three components ceramide/cholesterol/behenic acid (volume fraction ratio 53:10:37) in each bilayer after spin coating, the water content in head group and tail group regions were then calculated and are shown in Table 5. The percentage of water in the hydrophobic tail region necessary to fit the data is partially attributed to the defects, *e.g.* holes, present in the lamellar structures. As the temperature increases from 25 °C to 40 °C, the thickness of the tail group region decreases from 41.5 Å to 40.0 Å and the water content increases from 20% to 31% for the head group region, from 17% to 30% for the tail group region. Upon addition of cholesterol and behenic acid, although the layered structure of the deposited film becomes better defined, the bilayers become more fluid as a result of the kinks introduced by the cholesterol and hence the weaker intermolecular forces. Therefore, they are more susceptible to changes in temperature. Upon heating, the hydrocarbon chains become less ordered (less straight), resulting in decrease in thickness of the tail regions. At the same time, it is easier for the water molecules (D_2O) to penetrate the less ordered structure, leading to the increase in *Nb* of both head group and tail group regions. Another reason for the increase in *Nb* could be that high temperature facilitates the diffusion of water molecules through the bilayers. This was not observed for the pure ceramide lipid multi-bilayers could be because there are a lot more defects present in its structure and therefore the water molecules can readily diffuse and penetrate through the whole film even at low temperature.

Interaction of nanogels with mixed ceramide/cholesterol/behenic acid multi-bilayers

Since the mixed ceramide/cholesterol/behenic acid multi-bilayers are not stable with temperature, their interaction with nanogels was studied at a temperature close to physiological temperature, 35 °C. The reflectivity profiles measured before and after the addition of nanogel are shown in Fig. 5. Three nanogels (10% MBA, 20% MBA and 30% MBA) with different percentages of cross-linker were studied. The best fits are shown by solid lines in Fig. 5. The corresponding *Nb* profiles are shown in Fig. S5. The fitted parameters are given in Table 6. It can be seen that up to 38 bilayers in total could be deposited on the Si substrate.

The *Nb* values of both head group and tail group regions increase upon the addition of nanogels for all the three samples. This increase in *Nb* is caused by the depletion of the mixed lipids by the nanogels followed by the penetration of water (D_2O) and the possible introduction of solvated nanogels and nanogel-lipid complexes into the lipid bilayers, similar to the case of pure ceramide lipid multi-bilayers. The sample with 30% MBA nanogel results in the greatest increase in *Nb* (by 0.35×10^{-6} Å^{-2} for head group region, 0.6×10^{-6} Å^{-2} for tail group region) which suggests its strongest ability to deplete the mixed lipids. The increases in *Nb* values of the system with 20% MBA nanogels are 0.1×10^{-6} Å^{-2} (head group region) and 0.2×10^{-6} Å^{-2} (tail group region), and with 10% MBA nanogels are 0.05×10^{-6} Å^{-2} (head group region) and 0.15×10^{-6} Å^{-2} (tail group region). These results strongly support the conclusion obtained from the pure ceramide lipid multi-bilayers studies which suggests that the ability of nanogels to associate with lipids to form complexes follows the sequence of 30% MBA > 20% MBA > 10% MBA.

The water contents were calculated with the assumption that the mixed lipids of ceramide/cholesterol/behenic acid were depleted in the ratio of 1:0.3:1, therefore these three components in bilayers are kept constant at 1:0.3:1 (*i.e.* a volume fraction ratio of 53:10:37) after the addition of nanogels. However, the obtained results (Table 6) show that the water content of the tail group region is approaching approximately the same as that of the head group region. With 20% MBA nanogel the water content of the tail group region even exceeds that of the head group region, which is less likely to occur because head groups are more hydrophilic. Therefore, the assumption that the molar ratio of the three components after the addition of nanogels is 1:0.3:1 is not valid. The fact that behenic acid has the most positive *Nb* value for the head group and the most negative *Nb* value for the

tail group (Table 1), allows concluding that behenic acid is the main component that is first depleted by nanogels. This behaviour is consistent with the one observed for the same nanogels interacting with lipid monolayer [25]. Furthermore the decrease of the tail group region only observed with 30% MBA nanogels is evidence of its stronger ability to associate with and deplete skin lipids than its less crosslinked counterparts (10% MBA, 20% MBA).

4.4. The effect of penetration enhancer on the interaction of nanogels with mixed ceramide/cholesterol/behenic acid multi-bilayers

Previous studies [39–41] suggested that water soluble benzyl alcohol can readily partition into lipid bilayers where it is known to orient itself with its hydroxyl group in the head group region (polar region) and its aromatic nucleus directed into the tail group region (apolar core) of the bilayer. When intercalated into a lipid bilayer, benzyl alcohol acts as a membrane fluidizer, increasing the fluidity and decreasing the lipid base transition temperature. Therefore, benzyl alcohol can perturb and alter the multi-bilayers conformation which facilitates the passing and diffusion of foreign molecules. Prior to the study of the effect of benzyl alcohol as penetration enhancer on the interaction between nanogels and mixed lipid multi-bilayers, the influence of benzyl alcohol on the mixed lipid multi-bilayers structure was evaluated at 35 °C, close to physiological temperature. The normalized reflectivity profiles for multi-bilayers in the absence and presence of benzyl alcohol as a function of time are shown in Fig. 6. It was found that the impact of benzyl alcohol on the mixed lipid multi-bilayers is time dependent. The best fits are shown by solid lines. The corresponding *Nb* profiles are shown in Fig. S6. The parameters used to fit the reflectivity profiles are given in Table 7. It can be seen that upon addition of benzyl alcohol the *Nb* value of head group and tail group regions increases by 0.07×10^{-6} Å^{-2} & 0.2×10^{-6} Å^{-2} after 1 h, and by 0.2×10^{-6} Å^{-2} and 0.45×10^{-6} Å^{-2} after 3.5 h, respectively.

The observed increase in the *Nb* of both head and tail group regions is believed to be the result of enhanced penetration of D_2O into the bilayers. The time dependence of *Nb* indicates that the penetration of benzyl alcohol is not an instant but rather a slow process. Since the insertion of benzyl alcohol into the bilayers disorders the packing of the lipids, especially the hydrocarbon chains which become less packed and straight, the thickness of the tail group region shows a slight decrease (Table 7).

The effect of benzyl alcohol on the interaction of nanogels with mixed lipid multi-bilayers was then investigated at 35 °C using 30% MBA nanogels. The normalised reflectivity profiles of multi-bilayers in the presence of 30% MBA measured before and after the addition of benzyl alcohol as a function of time are shown in Fig. 7, together with the fittings (solid lines). The corresponding *Nb* profiles are shown in Fig. S7 and the parameters used to fit the r profiles are given in Table 8.

The results show that the *Nb* of both head and tail group regions increases with time after the addition of benzyl alcohol. The increments are 0.15×10^{-6} Å^{-2} and 0.3×10^{-6} Å^{-2} after 1 h, and 0.4×10^{-6} Å^{-2} & 0.6×10^{-6} Å^{-2} after 3.5 h respectively. The increments caused solely by the penetration of benzyl alcohol are 0.07×10^{-6} Å^{-2} and 0.2×10^{-6} Å^{-2} after 1 h and 0.2×10^{-6} Å^{-2} and 0.45×10^{-6} Å^{-2} after 3.5 h respectively (see Table 7) which are smaller than the increments in the presence of 30MBA nanogels. Therefore, the extra increments of *Nb* are caused by the further depletion of mixed lipids by the nanogels upon the addition of benzyl alcohol, followed by the introduction of D_2O into the bilayers. This promoted ability of nanogels to deplete mixed lipids results from the disordered multi-bilayers packing and the weakened attraction between neighbouring molecules upon the intercalation of benzyl alcohol into the bilayers which encourages the association between nanogels and lipids.

The overall outcome of these experiments is summarised schematically in Fig. 8. It highlights the fact that cholesterol enhances the lipids bilayer structural rigidity. The number of defects (voids) created in the multi-bilayer structure increases as the temperature increases below VPTT. This is because of increases in the degree of nanogels hydrophobicity as a result of loss of hydration shells. The tendency of some of bilayer fatty acids to reside in the bulk solution, previously reported (25), results in the complex formation and a further increase in the degree of the hydrophobicity of nanogels and their ability to solubilise lipids at the interface exposed to water. The introduction of an enhancer further aids this solubilisation process resulting in large numbers of voids and holes facilitating the diffusion of nanogels into the multilayer lipids structures.

5. Conclusion

The interactions of nanogels with both ceramide and mixed ceramide/cholesterol/behenic acid (molar ratio 1:0.3:1) lipid multi-bilayers, a more idealised representation of the skin composition, were investigated at the Si-water interface. The studies demonstrated the role of cholesterol and fatty acids in contributing to the increased ordering of the lipid multi-bilayers. The ability of nanogels to interact with both lipid multi-bilayers increased with the percentage of crosslinker (MBA). In the case of ceramide lipid multi-bilayers, this interaction was found to increase with temperature. Given that increases in cross-linker content and temperature result in nanogels with higher degree of hydrophobicity, it can be concluded that the nanogels associate with skin lipid molecules mainly through hydrophobic interactions.

Fatty acids play a role in facilitating membrane transport. The data obtained in this work support the hypothesis that behenic acid is the main component that is first depleted by nanogels. However given the limited solvent contrast that was used in the experiments, further work using additional contrasts are required to definitively confirm this. An alternative explanation of the observed enhancement effect is that it is the result of weakened neighbouring molecules interactions and the changes in the conformation of lipid bilayers, upon intercalation of benzyl alcohol into the bilayers. This work provides important advances in understanding the mechanism by which NIPAM based nanogels are able to interact with multi-bilayers, which can ultimately contribute to the development of novel nanoparticles able to interact and penetrate biological barriers.

Acknowledgement

The authors wish to thank the ISIS, STFC, UK, for beam time on SURF and INTER (RB 1410123). The European Commission (FP7 Marie Curie Actions, projects NANODRUG (MCITN-2011-289554) and NANOLEM (PIEF-GA-2013-627146)), the Chinese Scholarship Council and Queen Mary, University of London are gratefully acknowledged for financial support.

Appendix A. Supplementary material

Supplementary data to this article can be found online at https://doi.org/10.1016/j.jcis.2018.10.086.

References

[1] B. Baroli, Penetration of nanoparticles and nanomaterials in the skin: fiction or reality?, J. Pharm. Sci. 99 (1) (2010) 21–50.
[2] A. Naik, Y.N. Kalia, R.H. Guy, Transdermal drug delivery: overcoming the skin's barrier function, Pharm. Sci. Technol. Today 3 (9) (2000) 318–326.
[3] H. Bysell, R. Månsson, P. Hansson, M. Malmsten, Microgels and microcapsules in peptide and protein drug delivery, Adv. Drug Deliv. Rev. 63 (13) (2011) 1172–1185.
[4] M. Malmsten, H. Bysell, P. Hansson, Biomacromolecules in microgels—opportunities and challenges for drug delivery, Curr. Opin. Coll. Interf. Sci. 15 (6) (2010) 435–444.
[5] J.K. Oh, R. Drumright, D.J. Siegwart, K. Matyjaszewski, The development of microgels/nanogels for drug delivery applications, Prog. Polym. Sci. 33 (4) (2008) 448–477.
[6] D. Das, P. Ghosh, A. Ghosh, C. Haldar, S. Dhara, A.B. Panda, S. Pal, Stimulus-responsive, biodegradable, biocompatible, covalently cross-linked hydrogel based on dextrin and poly (N-isopropylacrylamide) for in vitro/in vivo controlled drug release, ACS Appl. Mater. Interf. 7 (26) (2015) 14338–14351.
[7] A. Saikia, S. Aggarwal, U. Mandal, Preparation and controlled drug release characteristics of thermoresponsive PEG/poly (NIPAM-co-AMPS) hydrogels, Int. J. Polymer. Mater. 62 (1) (2013) 39–44.
[8] D. Schmaljohann, Thermo-and pH-responsive polymers in drug delivery, Adv. Drug Deliv. Rev. 58 (15) (2006) 1655–1670.
[9] L. Zha, B. Banik, F. Alexis, Stimulus responsive nanogels for drug delivery, Soft Matter 7 (13) (2011) 5908–5916.
[10] V.C. Lopez, J. Hadgraft, M. Snowden, The use of colloidal microgels as a (trans) dermal drug delivery system, Int. J. Pharm. 292 (1) (2005) 137–147.
[11] V.C. Lopez, S. Raghavan, M. Snowden, Colloidal microgels as transdermal delivery systems, React. Funct. Polym. 58 (3) (2004) 175–185.
[12] N.A. Samah, N. Williams, C.M. Heard, Nanogel particulates located within diffusion cell receptor phases following topical application demonstrates uptake into and migration across skin, Int. J. Pharm. 401 (1) (2010) 72–78.
[13] N.H.A. Samah, C.M. Heard, Enhanced in vitro transdermal delivery of caffeine using a temperature-and pH-sensitive nanogel, poly (NIPAM-co-AAc), Int. J. Pharm. 453 (2) (2013) 630–640.
[14] G.S.L. Singka, N.A. Samah, M.H. Zulfakar, A. Yurdasiper, C.M. Heard, Enhanced topical delivery and anti-inflammatory activity of methotrexate from an activated nanogel, Eur. J. Pharm. Biopharm. 76 (2) (2010) 275–281.
[15] R. Pelton, Temperature-sensitive aqueous microgels, Adv. Coll. Interf. Sci. 85 (1) (2000) 1–33.
[16] J. Hadgraft, Skin deep, Eur. J. Pharm. Biopharm. 58 (2) (2004) 291–299.
[17] W. Kern, The evolution of silicon wafer cleaning technology, J. Elcetrochem. Soc. 137 (1990) 1887–1892.
[18] H. Trommer, R. Neubert, Overcoming the stratum corneum: the modulation of skin penetration, Skin Pharmacol. Physiol. 19 (2) (2006) 106–121.
[19] U. Mennicke, T. Salditt, Preparation of solid-supported lipid bilayers by spin-coating, Langmuir 18 (21) (2002) 8172–8177.
[20] F. Foglia, M. Lawrence, D. Barlow, Studies of model biological and bio-mimetic membrane structure: reflectivity vs diffraction, a critical comparison, Curr. Opin. Coll Interface Sci. (2015).
[21] M. Kiselev, Methods for lipid nanostructure investigation at neutron and synchrotron sources, Phys. Part. Nucl. 42 (2) (2011) 302.
[22] S. Krueger, Neutron reflection from interfaces with biological and biomimetic materials, Curr. Opin. Coll. Interf. Sci. 6 (6) (2001) 111–117.
[23] J. Penfold, K. Thomas, R. Neutron, reflectivity and small angle neutron scattering: an introduction and perspective on recent progress, Curr. Opin. Coll. Interf. Sci 19 (3) (2014) 198–206.
[24] H.P. Wacklin, Neutron reflection from supported lipid membranes, Curr. Opin. Coll. Interf. Sci. 15 (6) (2010) 445–454.
[25] L. Perino-Gallice, G. Fragneto, U. Mennicke, T. Salditt, F. Rieutord, Dewetting of solid-supported multilamellar lipid layers, Eur. Phys. J. E 8 (3) (2002) 275–282.
[26] H. Sun, M. Resmini, Zarbakhsh, J. Coll. Interf. Sci. 519 (2018) 97–106.
[27] P. Mills, B. Magnusson, S. Cross, Effect of solute lipophilicity on penetration through canine skin, Aust. Vet. J. 81 (12) (2003) 752.
[28] S.C. Maddock, P. Pasetto, M. Resmini, Novel imprinted soluble microgels with hydrolytic catalytic activity, Chem. Commun. 5 (2004) 536–537.
[29] J. Mueller, A. Schroeter, R. Steitz, M. Trapp, R.H.H. Neubert, Preparation of a New oligolamellar stratum corneum lipid model, Langmuir 32 (2016) 4673–4680.
[30] J.P. Patterson, A.M. Sanchez, N. Petzetakis, T.P. Smart, T.H. Epps III, I. Portman, N.R. Wilson, R.K. O'Reilly, A simple approach to characterizing block copolymer assemblies: graphene oxide supports for high contrast multi-technique imaging, Soft Matter 8 (12) (2012) 3322–3328.
[31] J. Penfold, R. Richardson, A. Zarbakhsh, J. Webster, D. Bucknall, A. Rennie, R. Jones, T. Cosgrove, R. Thomas, J. Higgins, Recent advances in the study of chemical surfaces and interfaces by specular neutron reflection, J. Chem. Soc., Faraday Trans. 93 (22) (1997) 3899–3917.
[32] J. Webster, S. Langridge, R. Dalgliesh, T. Charlton, Reflectometry techniques on the second target station at ISIS: methods and science, European Phys. J. Plus 126 (11) (2011) 1–5.
[33] N. Graham, A. Cameron, Nanogels and microgels: the new polymeric materials playground, Pure Appl. Chem. 70 (6) (1998) 1271–1275.
[34] J. Zhang, R. Pelton, Poly(N-isopropylacrylamide) microgels at the air-water interface, Langmuir 15 (23) (1999) 8032–8036.
[35] J. Generosi, C. Castellano, D. Pozzi, A. Castellano, X-ray and neutron reflectivity study of solid-supported lipid membranes prepared by spin coating, J. Appl. Phys. 96 (11) (2004) 6839–6844.
[36] A. Simonsen, L. Bagatolli, Structure of spin-coated lipid films and domain formation in supported membranes formed by hydration, Langmuir 20 (22) (2004) 9720–9728.
[37] T. Salditt, C. Li, A. Spaar, U. Mennicke, X-ray reflectivity of solid-supported, multilamellar membranes, Eur. Phys. J. E 7 (2) (2002) 105–116.
[38] J. Bouwstra, G. Gooris, K. Cheng, A. Weerheim, W. Bras, M. Ponec, Phase behavior of isolated skin lipids, J. Lipid Res. 37 (5) (1996) 999–1011.
[39] Y. Salinas, A.M. Castilla, M. Resmini, An L-proline based thermoresponsive and pH-switchable nanogel as a drug delivery vehicle, Polym. Chem. 9 (17) (2018) 2271–2280.
[40] C. Colley, J. Metcalfe, The localisation of small molecules in lipid bilayers, FEBS Lett. 24 (3) (1972) 241–246.
[41] K. Warner, S. Li, N. He, T. Suhonen, D. Chantasart, D. Bolikal, W. Higuchi, Structure–activity relationship for chemical skin permeation enhancers: probing the chemical microenvironment of the site of action, J. Pharm. Sci. 92 (6) (2003) 1305–1322.